# Symplectic algorithms for simulations of rigid-body systems using the exact solution of free motion

Ramses van Zon and Jeremy Schofield

*Chemical Physics Theory Group, Department of Chemistry, University of Toronto, 80 Saint George Street, Toronto, Ontario, Canada M5S 3H6*

Elegant integration schemes of second and fourth order for simulations of rigid-body systems are presented which treat translational and rotational motion on the same footing. This is made possible by a recent implementation of the exact solution of free rigid-body motion. The two schemes are time reversible and symplectic, and exactly respect conservation principles for both the total linear and the angular momentum vectors. Simulations of simple test systems show that the second-order scheme is stable and conserves all constants of the motion to high precision. Furthermore, the schemes are demonstrated to be more accurate and efficient than existing methods, except for high densities, in which case the second-order scheme performs at least as well, showing their general applicability. Finally, it is demonstrated that the fourth-order scheme is more efficient than the second-order scheme provided the time step is smaller than a system-dependent threshold value.

## I. INTRODUCTION

Systems of rigid bodies can be used to model phenomena on a wide range of length scales, from the dynamics of molecules [1–4], polymers, and other complex systems [5] to robotics on a macroscopic level [6]. On even larger scales, many astrophysical objects such as planets, satellites, and spacecraft can be regarded as rigid bodies [7,8]. Much recent work has been devoted to devising time-reversible and symplectic numerical integrators for rigid systems [1,2,8,9]. In this paper, we present second- and fourth-order symplectic integration schemes for general interacting rigid bodies that make use of a recent numerical implementation of the exact solution of free rigid bodies [10]. The schemes do not require specifying orientational parameters such as Euler angles, nor extending the state space, nor the use of quaternions and constraint conditions, and have a symplectic structure on the standard phase space of rigid systems. Besides being aesthetically appealing, the schemes are more efficient at a given level of accuracy in many cases, and never less efficient. Thus they are good multipurpose integrators.

The paper is structured as follows. In Sec. II the dynamics of rigid-body systems is briefly reviewed. The algorithms that apply to such systems are proposed in Sec. III, while their symplecticity is demonstrated in Sec. IV. Section V contains numerical tests on three model systems: a free asymmetric rotating body (Sec. V A), a water molecule in an electric field (Sec. V B), and a model of liquid water (Sec. V C). The paper ends with the conclusions in Sec. VI.

## II. DYNAMICS OF RIGID-BODY SYSTEMS

Consider a system consisting of $N$ rigid bodies, where each body $i$ has a mass $m_i$ and is described by its center-of-mass position $\mathbf{q}_i$ and its attitude matrix $\mathsf{A}_i$. The rows of $\mathsf{A}_i$ are the directions of the principal axes of the body in the laboratory frame. The position of a point $\alpha$ with coordinates $\tilde{\mathbf{r}}_\alpha$ in the principal axis frame of body $i$ is given by $\mathbf{r}_\alpha = \mathbf{q}_i + \mathsf{A}_i^T \tilde{\mathbf{r}}_\alpha$. In addition, each body has momentum

$$\mathbf{p}_i = m_i \dot{\mathbf{q}}_i \tag{1}$$

and angular velocity $\boldsymbol{\omega}_i$. In index notation, $\boldsymbol{\omega}_i$ is related to the time derivative of the attitude matrix via [10]

$$\sum_{a=x,y,z} \varepsilon_{bac}(\boldsymbol{\omega}_i)_a = \sum_{a=x,y,z} (\dot{\mathsf{A}}_i)_{ab}(\mathsf{A}_i)_{ac}, \tag{2}$$

where $\varepsilon_{bac}$ is the Levi-Civita symbol [11]. A related quantity is the angular momentum $\mathbf{L}_i = \mathsf{I}_i \boldsymbol{\omega}_i$, whose importance lies in the fact that the total angular momentum $\mathbf{L}_T = \Sigma_i(\mathbf{q}_i \times \mathbf{p}_i + \mathbf{L}_i)$ is a conserved quantity in rotationally symmetric systems. Here, $\mathsf{I}_i$ is the moment of inertia tensor $\mathsf{I}_i = \mathsf{A}_i^T \tilde{\mathsf{I}}_i \mathsf{A}_i$, where $\tilde{\mathsf{I}}_i = \mathrm{diag}(I_{ix}, I_{iy}, I_{iz})$ and $I_{ix}$, $I_{iy}$, and $I_{iz}$ are the principal moments of inertia.

The dynamics of the system is given by [11]

$$\dot{\mathbf{p}}_i = \mathbf{F}_i, \quad \dot{\mathbf{L}}_i = \boldsymbol{\tau}_i, \tag{3}$$

where the forces $\mathbf{F}_i$ and torques $\boldsymbol{\tau}_i$ are assumed to be functions of $\{\mathbf{q}_j\}$ and $\{\mathsf{A}_j\}$ only. The forces may derive from an interaction potential $V$ between sites, such that the force on site $\alpha$ of body $i$ is $\mathbf{F}_{i\alpha} = -\partial_{\mathbf{r}_{i\alpha}} V$. These forces then determine the body forces and torques:

$$\mathbf{F}_i = \sum_{\alpha=1}^{n_i} \mathbf{F}_{i\alpha}, \quad \boldsymbol{\tau}_i = \sum_{\alpha=1}^{n_i} (\mathbf{r}_{i\alpha} - \mathbf{q}_i) \times \mathbf{F}_{i\alpha}, \tag{4}$$

where $n_i$ is the number of interaction sites on body $i$.

## III. INTEGRATION ALGORITHMS

The proposed algorithm to integrate Eqs. (1)–(3) is based on the exact solution of torque-free dynamics and will be presented first, after which its derivation will be given.

In the algorithm, each body $i$ is specified by the set $(\mathbf{q}_i, \mathbf{p}_i, \mathsf{A}_i, \mathbf{L}_i)$, and two different evolution operators are defined. The first is the exact free evolution operator $\varphi_h^{(0)}$ over a time $h$, under which $\mathbf{L}_i$ and $\mathbf{p}_i$ are invariant while $\mathbf{q}_i$ and $\mathsf{A}_i$ evolve according to

$$\varphi_h^{(0)}\mathbf{q}_i = \mathbf{q}_i + h\mathbf{p}_i/m_i, \quad \varphi_h^{(0)}\mathbf{A}_i = \mathsf{P}_i(h)\mathbf{A}_i, \tag{5}$$

where the matrix $\mathsf{P}_i(h)$ (specified below) propagates $\mathbf{A}_i$ from time $t$ to $t_* = t+h$. The second evolution operator, denoted by $\varphi_h^{(1)}$, evolves the momenta due to interactions:

$$\varphi_h^{(1)}\mathbf{p}_i = \mathbf{p}_i + h\mathbf{F}_i, \quad \varphi_h^{(1)}\mathbf{L}_i = \mathbf{L}_i + h\boldsymbol{\tau}_i, \tag{6}$$

while $\mathbf{q}_i$ and $\mathbf{A}_i$ remain unchanged. Before applying this operator, the forces and torques must be computed using standard techniques [12,13].

In the integration schemes, the evolution over a time $t$ is replaced by evolution over $t/h$ time steps of duration $h$. In each time step, the two evolution operators $\varphi^{(0)}$ and $\varphi^{(1)}$ are applied in sequence. For the second-order integrator, this sequence is that of a generalized Verlet scheme, i.e.,

$$\varphi_{h/2}^{(1)}\varphi_h^{(0)}\varphi_{h/2}^{(1)} + O(h^3). \tag{7}$$

This scheme will be referred to as symplectic integrator using exact rotation matrices (SIER2).

For the fourth-order variant of the integrator, denoted as SIER4, the extended Forest-Ruth-like scheme of Omelyan *et al.* [14] is used, in which the true evolution is replaced by

$$\varphi_{h_1}^{(1)}\varphi_{h_2}^{(0)}\varphi_{h_3}^{(1)}\varphi_{h_4}^{(0)}\varphi_{h_5}^{(1)}\varphi_{h_4}^{(0)}\varphi_{h_3}^{(1)}\varphi_{h_2}^{(0)}\varphi_{h_1}^{(1)} + O(h^5), \tag{8}$$

with $h_4 = h/2 - h_2$, $h_5 = h - 2(h_1 + h_2)$, $h_1 = 0.172\,086\,559\,029\,514\,3h$, $h_2 = 0.591\,562\,030\,755\,156\,8h$, and $h_3 = -0.161\,621\,762\,210\,722\,2h$.

The most unusual aspect of these integrators is the use of the exact solution of $\mathsf{P}_i$ in $\varphi^{(0)}$ [15]. Its form is [10]

$$\mathsf{P}(h) = \mathsf{R}_1(\widetilde{\mathbf{L}}_*)\mathsf{R}_2(\psi)\mathsf{R}_1^T(\widetilde{\mathbf{L}}), \tag{9}$$

where the $i$ dependence has been dropped with the understanding that each body $i$ has its own matrix $\mathsf{P}_i$ to propagate its specific attitude matrix $\mathbf{A}_i$. In Eq. (9), $\widetilde{\mathbf{L}} = \mathbf{A}\mathbf{L}$ is the angular momentum in the principal axes frame at time $t$, $\widetilde{\mathbf{L}}_*$ is the same quantity at time $t_*$, and $\mathsf{R}_1$ is

$$\mathsf{R}_1(\widetilde{\mathbf{L}}) = \frac{1}{LL_\perp}\begin{pmatrix} \widetilde{L}_x\widetilde{L}_z & -L\widetilde{L}_y & L_\perp\widetilde{L}_x \\ \widetilde{L}_y\widetilde{L}_z & -L\widetilde{L}_x & L_\perp\widetilde{L}_y \\ -L_\perp^2 & 0 & L_\perp\widetilde{L}_z \end{pmatrix},$$

with $L_\perp = (\widetilde{L}_x^2 + \widetilde{L}_y^2)^{1/2}$ and $L = |\widetilde{\mathbf{L}}|$. While $\widetilde{\mathbf{L}}$ is known at the start of the time step, $\widetilde{\mathbf{L}}_*$ can be computed from the free solution of the Euler equations [8,10], which involve Jacobi elliptic functions. Fortunately, efficient routines are available to evaluate such functions [16].

The matrix $\mathsf{R}_2(\psi)$ in Eq. (9) is a rotation around the $z$ axis by an angle [10]

$$\psi = \alpha h + \alpha c \int_t^{t_*} w(s)ds, \tag{10}$$

with $\alpha = L/I_z$, $w(s) = L^2/L_\perp^2(s)$, $c = 2I_zE/L^2 - 1$, where $E = \mathbf{L}\cdot\mathsf{I}^{-1}\mathbf{L}/2$.

The explicit solution of the integral in Eq. (10) requires the evaluation of elliptic integrals and $\vartheta$ functions [10], which can become somewhat of a computational burden

[17]. Instead, standard numerical approaches could be used, such as quadrature-based methods. However, quadrature-based methods involve evaluating additional elliptic functions at several intermediate points in the interval $(t, t_*)$. The following method of numerically computing the integral does not suffer from this drawback.

For small time steps $h$, the integral in Eq. (10) can be expressed using the integral of the polynomial approximation of the integrand $w(s)$ found by Hermite interpolation [18], yielding

$$\int_t^{t_*} w(s)ds = \sum_{j=1}^n \frac{n!\,(2n-j)!\,h^j}{j!\,(n-j)!\,(2n)!}[w^{(j-1)} + (-)^{j-1}w_*^{(j-1)}], \tag{11}$$

plus corrections of $O(h^{2n+1})$. Here, $w^{(j)} = d^j w(t)/dt^j$ and $w_*^{(j)} = w^{(j)}(t_*)$. In the present case, $w^{(j)}$ and $w_*^{(j)}$ can be expressed in terms of $\widetilde{\mathbf{L}}$ and $\widetilde{\mathbf{L}}_*$, respectively, using the Euler equations recursively. To be more precise,

$$w^{(1)} = \frac{2(I_x - I_y)\widetilde{L}_x\widetilde{L}_y\widetilde{L}_z}{I_xI_yL^2}w^2,$$

while in general

$$w^{(j)} = S_j(w) \times \begin{cases} \alpha^j & \text{if } j \text{ is even,} \\ w^{(1)}\alpha^{j-1} & \text{if } j \text{ is odd,} \end{cases}$$

where the $S_j(w)$ are polynomials in $w$. The first few are $S_0 = w$, $S_1 = 1$, and $S_2 = 2a + 4(bc-a)w + 6(c-b)cw^2 - 8c^2w^3$, where $a = (I_z/I_y - 1)(I_z/I_x - 1)$ and $b = 2 - I_z/I_y - I_z/I_x$. The $S_j$ satisfy the recursion $S_j = S_{j-1}dh_j/dw + 2h_jdS_{j-1}/dw$ with $h_j = 2w(1-w)(a+bcw+c^2w^2)$ for even $j$, and $S_j = dS_{j-1}/dw$ for odd $j$ [19].

Since odd time derivatives change sign under time reversal, each term in Eq. (11) is invariant under time reversal, so this approximation preserves the time reversibility of the integrators. By increasing $n$ until $\psi$ has converged, one obtains a "numerically exact" result.

It should be remarked that the equations above apply if $2E > I_yL^2$. Otherwise, one must perform a rotation $\mathsf{U}^*$ in the principal axes frame to exchange the $x$ and $z$ directions and reverse the $y$ direction [10].

## IV. SYMPLECTICITY

It is clear that Eqs. (5)–(7) generalize the Verlet integration algorithm to rigid systems. But it is not obvious that this integrator [or the higher-order variant in Eq. (8)] is symplectic, since symplecticity is a property of the equations of motion in Hamiltonian mechanics. In this formulation [11], the state of the system is described by generalized coordinates and momenta *conjugate* to these coordinates. The structure of the equations of motion is *symplectic* if $\dot{\boldsymbol{\Gamma}} = \mathsf{J}\partial_\Gamma\mathcal{H}$, where $\boldsymbol{\Gamma}$ is the phase point consisting of the generalized coordinates and momenta, and $\mathcal{H}$ is the Hamiltonian [11]. Here $\mathsf{J}$ is defined to be $\mathsf{J} = \begin{pmatrix} 0 & \mathbf{1} \\ -\mathbf{1} & 0 \end{pmatrix}$, where $\mathbf{1}$ is a $6N \times 6N$ unit matrix. For time-independent $\mathcal{H}$, the evolution over a time $h$ may

be written as $\mathbf{\Gamma}(h) = \exp[\hat{L}h]\mathbf{\Gamma}(0)$, where the Liouvillian $\hat{L} \equiv -\partial_{\mathbf{\Gamma}}\mathcal{H} \cdot \mathbf{J}\partial_{\mathbf{\Gamma}}$. The operator $\exp[\hat{L}h]$ is called the propagator and is symplectic due to the form of $\hat{L}$.

While there are several ways to parametrize the attitude matrix $\mathsf{A}$, three generalized coordinates are always required, denoted here by $\boldsymbol{\vartheta}_i = (\vartheta_{i1}, \vartheta_{i2}, \vartheta_{i3})$. From the Lagrangian of interacting rigid bodies $\mathcal{L} = \frac{1}{2}\Sigma_{i=1}^{N}(m_i|\dot{\mathbf{q}}_i|^2 + \boldsymbol{\omega}_i \cdot \mathsf{I}_i \boldsymbol{\omega}_i) - V(\{\mathbf{q}_j, \boldsymbol{\vartheta}_j\})$, one finds

$$\mathcal{H} = \frac{1}{2}\sum_i \left( \frac{|\mathbf{p}_i|^2}{m_i} + \boldsymbol{\pi}_i \cdot \mathsf{M}_i^{-1} \boldsymbol{\pi}_i \right) + V(\{\mathbf{q}_j, \boldsymbol{\vartheta}_j\}), \qquad (12)$$

where the generalized momenta are given by $\mathbf{p}_i = m_i\dot{\mathbf{q}}$ and $\boldsymbol{\pi}_i = \mathsf{M}_i\dot{\boldsymbol{\vartheta}}_i$. Here, $\mathsf{M}_i$ is a $\boldsymbol{\vartheta}_i$-dependent matrix given by $\mathsf{M}_i = \mathsf{N}_i\mathsf{I}_i\mathsf{N}_i^T$, where, in turn, $N_{ab} = \frac{1}{2}\varepsilon_{bcd}A_{ec}\partial A_{ed}/\partial\vartheta_a$. To derive the integration schemes (7) and (8), the Hamiltonian is split into $\mathcal{H}^{(1)} = V(\{\mathbf{q}_j, \boldsymbol{\vartheta}_j\})$ and $\mathcal{H}^{(0)} = \mathcal{H} - \mathcal{H}^{(1)}$. From the $\mathcal{H}^{(j)}$, the partial Liouvillians $\hat{L}^{(j)} = -\partial_{\mathbf{\Gamma}}\mathcal{H}^{(j)} \cdot \mathbf{J}\partial_{\mathbf{\Gamma}}$ and symplectic propagators $\exp[\hat{L}^{(j)}h]$ are constructed. The propagator $\exp[\hat{L}^{(0)}h]$ evolves the rigid system freely over a time $h$ and thus coincides with the propagator $\varphi_h^{(0)}$ in Eq. (5). The action of the propagator $\exp[\hat{L}^{(1)}h]$ on a phase point $\mathbf{\Gamma}$ can also be determined:

$$e^{\hat{L}^{(1)}h}(\mathbf{q}_i, \boldsymbol{\vartheta}_i, \mathbf{p}_i, \boldsymbol{\pi}_i) = (\mathbf{q}_i, \boldsymbol{\vartheta}_i, \mathbf{p}_i - h\partial_{\mathbf{q}_i}V, \boldsymbol{\pi}_i - h\partial_{\boldsymbol{\vartheta}_i}V),$$

from which it follows that [cf. Eq. (6)]

$$e^{\hat{L}^{(1)}h}\mathbf{L}_i = \mathbf{L}_i - h\mathsf{N}_i^{-1}\partial_{\boldsymbol{\vartheta}_i}V = \mathbf{L}_i + h\boldsymbol{\tau}_i = \varphi_h^{(1)}\mathbf{L}_i.$$

Hence both $\varphi_h^{(0)}$ and $\varphi_h^{(1)}$ are symplectic operators. Since a succession of symplectic operators is also symplectic, the SIER integrators in Eqs. (7) and (8) are symplectic. It is straightforward to show that SIER2 and SIER4 schemes are second and fourth order, respectively [12,14].

Both $\varphi_h^{(0)}$ in Eq. (5) and $\varphi_h^{(1)}$ in Eq. (6) *strictly* conserve the angular momentum vector $\mathbf{L}_T$ for spherically symmetric systems. The conservation of $\mathbf{L}_T$ under $\varphi_h^{(0)}$ arises because $\mathbf{L}_i$ is a constant of the exact free motion, whereas the equality $\varphi_h^{(1)}\mathbf{L}_T = \mathbf{L}_T$ is a consequence of the rotational invariance of the potential $V$. Due to translational invariance, the momentum $\Sigma_i\mathbf{p}_i$ is also conserved. Furthermore, the energy fluctuations are bounded due to the existence of a pseudo-Hamiltonian [12].

## V. NUMERICAL TESTS

### A. Free rotation of an asymmetric body

To demonstrate the advantage of the SIER integrators for an asymmetric body, simulations were performed on an isolated rigid body, whose moments of inertia are those of a water molecule, with initial conditions drawn from a canonical distribution at 297 K. For comparison, simulations were also performed using the scheme of McLachlan, Reich, Dullweber, and Leimkuhler (MRDL) [1,9] and the SEJ4 scheme of Ref. [8] (so named in that reference). The advantage of considering a free rigid body is that the exact motion is

known and can be used to measure the deviation in the trajectories in addition to checking violations of energy conservation. The energy is in fact insensitive to the orientation, and the violations of energy conservation turn out to be small for all the integration methods. To show that this does not mean that all methods are equally accurate, as an alternative error estimate, we used $\delta = \langle \frac{1}{6}\text{Tr}[(\mathsf{A} - \mathsf{A}_{\text{ex}})(\mathsf{A} - \mathsf{A}_{\text{ex}})^T]\rangle^{1/2}$, with $\mathsf{A}_{\text{ex}}$ the exact result [10]. While $\delta \approx 0$ for $\mathsf{A} \approx \mathsf{A}_{\text{ex}}$, $\delta = 1$ for a random rotation matrix $\mathsf{A}$. Numerically it is found that the error scales as $\delta = t/(10\tau)$ for moderate $t$, where $\tau$ is the time at which the error in $\mathsf{A}$ becomes 10%. Hence $\tau$ can be viewed as the time scale at which the orientation of the body is incorrectly calculated. This time scale depends on the time step $h$ and the scheme used. For $h = 1.66$ fs, the time scale at which the orientation becomes inaccurate is $\tau \approx 117$ ps using the MRDL scheme, while the SEJ4 scheme gives $\tau \approx 0.91$ $\mu$s, and the SIER2 method gives $\tau \approx 16$ ms (SIER2 and SIER4 have similar accuracy here). Given that in gases at standard conditions, typical free flight times are on the order of 100 ps, one might still consider the error in the MRDL result acceptable in such applications. However, time steps as large as 8 fs are possible for such systems [4]. For this time step, the time scale at which the orientation becomes inaccurate in the MRDL method is $\tau \approx 7.6$ ps. Thus, the orientation would be incorrectly given by the MRDL method well before a free flight is over, even though the violations in the energy conservation are small ($\sim 0.01\%$). Somewhat surprisingly, then, the time step that can be used in MRDL simulations of a low-density system is limited not by interaction parameters but by the accuracy of the free flight. On the other hand, the SEJ4 method gives $\tau \approx 2.1$ ns, and the SIER2 method gives $\tau \approx 48$ ms, so both give orientations that are still accurate after a free flight. In terms of computational load, for a fixed time step, the SIER2 computation was between 70% and 100% slower than the MRDL, while the SEJ4 computation was another 20% slower still. Thus SEJ4 is slower and less accurate than SIER2. And while MRDL is roughly twice faster for given $h$, this cannot make up for the loss in accuracy.

### B. Water molecule in an electric field

To test the SIER integrators on a nonfree body, a constant electric field of 2.7 MV/m directed along the $z$ axis is introduced with which the water molecule interacts via its dipole moment of 1.84 D. The strength of the electric field corresponds to that induced by a second water molecule at a distance of 7 Å. Since the exact motion of the molecule is not known for this case, more conventional measures for accuracy are used. In Table I, the rms fluctuations of two conserved quantities, the total energy $\mathcal{H}$ and the $z$ component of the angular momentum vector, $L_z$, are given for different time steps for the SIER integrators and compared with the MRDL scheme and the SEJ4 scheme. Note that the fluctuations of $\mathcal{H}$ are given relative to the fluctuations of the potential energy $\Delta V$ (a natural scale of energy fluctuations), while the fluctuations of $L_z$ are given relative to the average $L_z$. For an equitable comparison, the relative accuracies of the simulations were compared as a function of $h/f$, where $f$ is the

TABLE I. Conservation of $\mathcal{H}$ and $L_z$ for a dipole (1.84 D) in an electric field (2.7 MV/m), using various integrators.

| $h/f$ | $\Delta\mathcal{H}/\Delta V$ (%) | | | | $\Delta L_z/\langle L_z\rangle$ | | | |
|---|---|---|---|---|---|---|---|---|
| (fs) | MRDL | SEJ4 | SIER2 | SIER4 | MRDL $(10^{-13})$ | SEJ4 $(10^{-3})$ | SIER2 $(10^{-13})$ | SIER4 $(10^{-13})$ |
| 4.2 | $1.8\pm0.3$ | $0.088\pm0.006$ | $0.088\pm0.006$ | $0.0035\pm0.0005$ | $16\pm1$ | $0.0014\pm0.0003$ | $6\pm1$ | $2.6\pm0.7$ |
| 11 | $11.4\pm1.6$ | $0.55\pm0.04$ | $0.55\pm0.4$ | $0.27\pm0.06$ | $7.0\pm0.6$ | $0.069\pm0.019$ | $2.1\pm0.7$ | $1.8\pm0.3$ |
| 21 | $51\pm7$ | $2.24\pm0.16$ | $2.22\pm0.15$ | $14\pm2$ | $3.9\pm0.4$ | $2.3\pm1.1$ | $1.4\pm0.3$ | $2.6\pm0.4$ |

number of force evaluations per time step. For the MRDL, SEJ4, and SIER2 methods, $f=1$, while $f=4$ for the SIER4 computation. We note that the relative real-time computational loads are comparable to those in the free case.

It is evident from Table I that the SIER2 scheme has the same degree of energy conservation as SEJ4, outperforming MRDL in this respect. However, the SIER2 and MRDL methods conserve $L_z$ equally well since the MRDL scheme also conserves the angular momentum exactly. On the other hand, the conservation of $L_z$ in the SEJ4 scheme is orders of magnitude worse than the other propagation schemes, casting doubt on the accuracy of its rotational dynamics. Thus, SIER2 combines the excellent energy conservation of SEJ4 with the exact angular momentum conservation of MRDL. In addition, SIER4 improves the energy conservation for $h/f$ below a threshold value of about 12 fs.

### C. Liquid water

In simulations of high-density liquids, one expects the free flight to be less important, and the advantages of using the SIER method less. However, one still expects SIER4 to give better results than SIER2. To test this, simulations were also performed on a system of 512 water molecules at liquid density at a temperature of 297 K [20]. To ensure strict energy conservation, a smooth molecular cutoff of 11 Å was employed. For the simulations, time steps ranging from $h=0.1$ to 7 fs were used (above which one sees a substantial energy drift). The results for SIER2 and SIER4 simulations are shown in Fig. 1. MRDL and SEJ4 simulations were also performed, but their results as well as their real-time compu-

tational loads were virtually indistinguishable from those of SIER2, and therefore are not plotted in Fig. 1. Thus, from the perspective of energy conservation, SIER2 performs as well as MRDL and SEJ4 here, although the trajectories are likely to be more accurate (as in the free case). From Fig. 1, it is evident that below $h/f\approx1.8$ fs, SIER4 is more accurate than SIER2, although its theoretical scaling of $O(h^4)$ for small $h$ is frustrated by round-off errors [21].

### VI. CONCLUSIONS

In this paper, two symplectic, time-reversible algorithms for simulating rigid-body dynamics were presented, SIER2 and SIER4, which are of second and fourth order, respectively. The schemes do not use constraint conditions, nor an extended state space, nor Euler angles or quaternions, but instead make use of a recent implementation of the exact solution of free rigid-body motion. The integrators conserve the symplectic structure on the conventional phase space of rigid systems and respect conservation laws of linear and angular momentum exactly when applicable.

Numerical comparisons with two existing integration methods (MRDL and SEJ4) were performed for three systems: a free asymmetric rigid body, a water molecule in an external field, and liquid water. In the free case, a comparison with the exact trajectory was possible, which showed that the orientational dynamics given by the SIER schemes is superior to existing integration schemes at a given numerical cost. For the water molecule in an external field, the accuracy of the trajectories was assessed using the conserved quantities of energy and the $z$ component of the angular momentum. Here too, the SIER schemes performed better at a given numerical cost. For the simulation of water at liquid densities, the energy conservation of the SIER methods is equal to that of the other integrators, due to the dominance of the forces in the accumulated error. Nonetheless, the trajectories are likely to be more accurate, because the free motion step in the integrator is performed exactly.

The integrators presented here should be of use in astrophysical simulations in which accuracy is important as well as in simulations of biomolecular and other systems in chemical physics, which often require propagation of many degrees of freedom to long time scales.
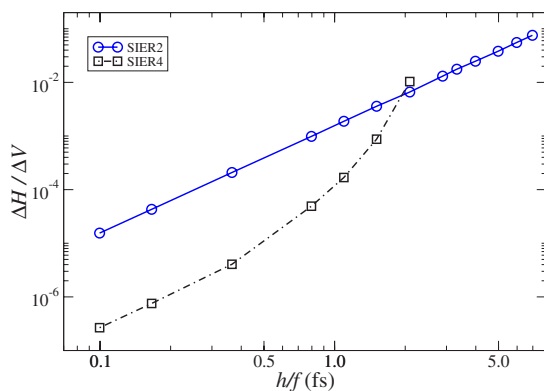


FIG. 1. (Color online) rms energy fluctuations using SIER2 and SIER4 for liquid water. All data are averaged over nine 1 ps runs divided by the fluctuations in the potential energy $\Delta V$.

[1] A. Dullweber, B. Leimkuhler, and R. McLachlan, J. Chem. Phys. **107**, 5840 (1997).

[2] T. Miller III *et al.*, J. Chem. Phys. **116**, 8649 (2002).

[3] L. Hernández de la Peña *et al.*, J. Chem. Phys. **126**, 074105 (2007).

[4] L. Hernández de la Peña *et al.*, J. Chem. Phys. **126**, 074106 (2007).

[5] M. P. Allen, D. Frenkel, and J. Talbot, Comput. Phys. Rep. **9**, 301 (1989); W. van Ketel, C. Das, and D. Frenkel, Phys. Rev. Lett. **94**, 135703 (2005).

[6] D. Baraff, Comput. Graphics **23**, 223 (1989).

[7] J. R. Wertz, in *Spacecraft Attitude Determination and Control*, edited by J. R. Wertz (Kluwer, Dordrecht, 1978), pp. 523–528.

[8] E. Celledoni and N. Säfström, J. Phys. A **39**, 5463 (2006).

[9] S. Reich, Fields Inst. Commun. **10**, 181 (1996); B. Leimkuhler and S. Reich, *Simulating Hamiltonian Dynamics* (Cambridge University Press, Cambridge, U.K., 2005).

[10] R. van Zon and J. Schofield, J. Comput. Phys. (to be published).

[11] H. Goldstein, *Classical Mechanics* (Addison-Wesley, Reading, MA, 1980).

[12] D. Frenkel and B. Smit, *Understanding Molecular Simulation* (Academic Press, San Diego, 1996).

[13] S. L. Price, A. J. Stone, and M. Alderton, Mol. Phys. **52**, 987 (1984).

[14] I. P. Omelyan, I. M. Mryglod, and R. Folk, Comput. Phys. Commun. **146**, 188 (2002); **151**, 272 (2003).

[15] Appendix C of Ref. [1] contains the Verlet-like scheme (7) for spherical or symmetric tops (without derivation).

[16] *Handbook of Mathematical Functions*, edited by M. Abramowitz and I. A. Stegun (Dover, New York, 1965).

[17] Special functions are not required for the spherically symmetric top, for which $c=0$, and the symmetric top, for which $cw =I_z/I_x-1$. In these cases, $\psi=hL/I_x$.

[18] G. M. Philips, BIT Numer. Math. **13**, 177 (1973).

[19] An implementation of the integrator along these lines can be found at http://www.chem.utoronto.ca/staff/JMS/rigidrotor.html

[20] W. L. Jorgensen, J. Chandrasekhar, J. D. Madura, R. W. Impey, and M. L. Klein, J. Chem. Phys. **79**, 926 (1983).

[21] See, e.g., R. D. Skeel, Appl. Numer. Math. **29**, 3 (1999); T. Fukushima, Astron. J. **121**, 1768 (2001).